Check for updates

The FEBS Journal

FEBS PRESS science publishing by scientists

Phosphorylation of BigH1 regulates its expression pattern and promotes embryonic development

Ramóna Pék[1,*], Aladár Pettkó-Szandtner[2], Anikó Szabó[1], Balázs Vedelek[1], Bence György Gombás[3], Zoltán Villányi[3], Péter Vilmos[1], Imre Miklós Boros[3,4], László Henn[1] and Gyula Timinszky[1]

1 Institute of Genetics, HUN-REN Biological Research Centre, Szeged, Hungary
2 Proteomics Research Group, Core Facility, HUN-REN Biological Research Centre, Szeged, Hungary
3 University of Szeged, Szeged, Hungary
4 Department of Biochemistry and Molecular Biology, Faculty of Science and Informatics, Institute of Biochemistry, HUN-REN Biological Research Centre, Szeged, Hungary

Keywords
BigH1; *Drosophila*; embryogenesis; linker histone; phosphorylation

Correspondence
G. Timinszky and L. Henn, Institute of Genetics, HUN-REN Biological Research Centre, Temesvári krt. 62, Szeged H-6726, Hungary
E-mail: timinszky.gyula@brc.hu and henn.laszlo@brc.hu

Present address
*CNRS, IGDR (Institut de Génétique et Développement de Rennes), UMR 6290, University of Rennes, France

Ramóna Pék and Aladár Pettkó-Szandtner equally contributing first authors.

(Received 4 February 2026, revised 30 June 2026, accepted 28 July 2026)

doi:10.1111/febs.70715

Metazoan genomes typically encode several linker histone variants, often expressed in a tissue- or developmental stage-specific manner. The *Drosophila melanogaster* genome contains only two linker histone variants: H1 is present in somatic cells, while BigH1 substitutes H1 in the germline and early embryos. In the early stages of embryogenesis, BigH1 is replaced by H1 in the chromatin of somatic cells, contributing to the initiation and maintenance of the zygotic gene expression program. Nevertheless, the molecular mechanism of this exchange and the possible functions of post-translational modifications of BigH1 in this process remain elusive. Here, we identify phosphorylation as a key post-translational regulator of BigH1 dynamics. Using proteomics and targeted mutagenesis of the endogenous *BigH1* locus, we show that the loss of N-terminal phosphorylation results in persistent retention of BigH1 in somatic nuclei throughout embryogenesis, indicating a failure in BigH1 turnover. In contrast, disruption of C-terminal phosphorylation does not markedly affect BigH1 clearance but increases defects during early nuclear divisions and compromises embryonic development, particularly under suboptimal conditions. Together, these findings demonstrate that domain-specific phosphorylation differentially regulates BigH1 function, coordinating its early embryonic role with its subsequent removal from the chromatin.

Introduction

Linker histones are essential for chromatin compaction and organization. By binding to the entry and exit points of DNA on the nucleosome, H1 stabilizes the nucleosome structure and facilitates the formation of higher-order chromatin [1,2]. H1 protein comprises three distinct domains: a central globular domain (GD), an N-terminal domain (NTD), and a C-terminal domain (CTD). The GD possesses a defined structure and directly interacts with DNA. In contrast, both the NTD and CTD are intrinsically disordered and enriched in lysine residues [3]. While the CTD also participates in DNA binding, the NTD is thought to have a regulatory role in DNA-binding affinity [4].

Abbreviations
AEL, after egg laying; CDK, cyclin-dependent kinase; CTD, C-terminal domain; GD, globular domain; IP, immunoprecipitation; MS, mass spectrometry; MZT, maternal-to-zygotic transition; NTD, N-terminal domain; PTM, post-translational modification; ZGA, zygotic genome activation.

© 2026 The Author(s). *The FEBS Journal* published by John Wiley & Sons Ltd on behalf of Federation of European Biochemical Societies.
This is an open access article under the terms of the Creative Commons Attribution License, which permits use, distribution and reproduction in any medium, provided the original work is properly cited.

Unlike core histones, linker histones exhibit greater evolutionary divergence, particularly in their variable N- and C-termini. This variation is reflected in the versatile expression of multiple H1 subtypes across different tissues and developmental stages of animals. For example, humans possess 11 H1 variants: seven are expressed in somatic cells (H1.1, H1.2, H1.3, H1.4, H1.5, H1.0, and H1.X), three are specific to the testis (H1t, T2, and HILS), and one is unique to oocytes (H1oo). Oocyte-specific H1s are common across many animal species, including *C. elegans* (H1.1/HIS-24), sea urchins (Cs-H1), *Xenopus laevis* (B4/H1M), zebrafish (H1M), and mice (H1oo). Oocyte-specific variants also govern zygotic development, and are then replaced by somatic H1s during early embryogenesis. The replacement of early embryonic linker histones may play a role in the reprogramming of nuclei through zygotic genome activation (ZGA) [1,5].

Drosophila melanogaster possesses only two linker histone variants: H1 and BigH1 [6]. The somatic linker histone H1 is encoded by approximately 100 identical gene copies within the histone gene cluster [7]. In contrast, BigH1 is a larger variant specified by a single locus and is expressed in the germline and early embryos. BigH1 plays a crucial role in ZGA and facilitates rapid replication cycles during early embryogenesis. During these shortened mitotic cycles at early development, the standard cell-cycle restriction points are bypassed, leading to an elevated accumulation of DNA damage [8]. Under these conditions, a Chk2-dependent mechanism serves to eliminate damaged nuclei during the rapid nuclear cleavages, a phenomenon called nuclear fallout [9–11]. Following ZGA, maternally deposited BigH1 is replaced by somatic H1 and thus disappears from somatic cells after gastrulation and only persists in primordial germ cells [6,12].

Post-translational modifications (PTMs) of H1 histones are vital for the regulation of chromatin folding and compaction [13,14]. Several types of PTMs occur on H1 proteins, such as acetylation, crotonylation, methylation, ubiquitylation, ADP-ribosylation, and formylation, but phosphorylation is the most common and well-known among all. Most of these PTMs are largely concentrated in the NTD and CTD; however, modifications within the GD have also been documented [14]. Cyclin-dependent kinase (CDK)-type phosphorylation sites or non-CDK sites in metazoan cells occur at both terminal domains of several H1 variants. CDK sites are phosphorylated in a cell-cycle-dependent manner: serine residues serve as primary phosphoacceptors during interphase, whereas threonine residues are preferentially phosphorylated during mitosis [15]. Evidence suggests that phosphorylation modulates CTD conformation, thereby altering its affinity for nucleosomes [16]. It has also been reported that the extent of H1 phosphorylation has different effects on chromatin condensation during metaphase, suggesting a functional role of H1 hyper-phosphorylation throughout the cell cycle [16,17].

It has been demonstrated that linker histone phosphorylation can induce both chromatin relaxation and condensation, and thus takes part in basic cellular processes, such as cell-cycle progression, DNA damage response, transcription, cell differentiation, and aging [18]. Moreover, impaired H1 phosphorylation is also associated with diseases, such as cancer and viral infections [13,14]. The mechanism by which H1 phosphorylation alters chromatin function is attributed to the reduction in the protein's net positive charge, thus weakening the electrostatic interaction with the nucleosomes. On the contrary, upon phosphorylation, the lysine-rich CTD is able to form a β-sheet-like structure, thereby increasing the binding affinity of H1 for chromatin [19].

Drosophila H1 is also phosphorylated, as was first demonstrated in 1971 by an electrophoretic method [20]. Decades later, mass-spectrometry (MS) experiments revealed S11 as the major phosphorylation site at the N terminus; however, other residues were identified at the NTD and GD as well [21,22]. Since H1 is encoded by one hundred identical gene copies, shedding light on the significance of H1 PTMs through mutational analysis is quite challenging. However, it has been shown that the S11A mutant H1 transgene exhibits slower H1 recovery than the wild-type protein in the FRAP assay. Nevertheless, this substitution does not appear to have a measurable effect on chromatin compaction [23].

In 2013, a second linker histone, BigH1, was identified in *Drosophila*, showing a germline- and early embryo-specific expression pattern. The putative phosphorylation of BigH1 was demonstrated in early embryos by western blot as a slow-migrating protein isoform with alkaline phosphatase sensitivity [6]. In contrast to H1, previous phosphoproteome results indicated that BigH1 phosphorylation sites were restricted to the CTD (at S287/S288, S299, and S331) [24]. Although there is clear evidence for phosphorylation of the embryonic linker histone, the functional significance of this PTM remained undetermined. Here, we demonstrate that BigH1 is subject to phosphorylation within both its NTD and CTD; furthermore, this PTM regulates its temporal expression

© 2026 The Author(s). *The FEBS Journal* published by John Wiley & Sons Ltd on behalf of Federation of European Biochemical Societies.

17424658, 0, Downloaded from https://febs.onlinelibrary.wiley.com/doi/10.1111/febs.70715 by HUN-REN Biological Research Center, Szeged, Wiley Online Library on [26/11/2026]. See the Terms and Conditions (https://onlinelibrary.wiley.com/terms-and-conditions) on Wiley Online Library for rules of use; OA articles are governed by the applicable Creative Commons License

pattern and is critical for proper embryonic development.

Results

BigH1 is phosphorylated at both the N- and C-terminal domains

To identify the phosphorylation sites of BigH1, we used FLAG-tag immunoprecipitation (IP) coupled with MS on 1–2-h-old *Drosophila* embryos expressing FLAG-tagged BigH1. In contrast to recent reports on *Drosophila* H1, where phosphorylation sites are predominantly located in the NTD [21,22], our MS–MS proteomics experiments revealed 16 possible phosphorylation sites on BigH1, most of which are located at the C terminus. We detected phosphorylation on T74 and S88 at the N terminus, and on S254, S255, T264/S265/T267, S299, S326/T327/S331, and T338/S339/T340 residues at the C terminus (Fig. 1A, Table 1. Fig. S1). Due to the complexity of the phosphorylation patterns and the inherent ambiguity of phosphosite localization when site-determining fragment ions are absent, some phosphorylation events could only be assigned to clusters of adjacent residues.

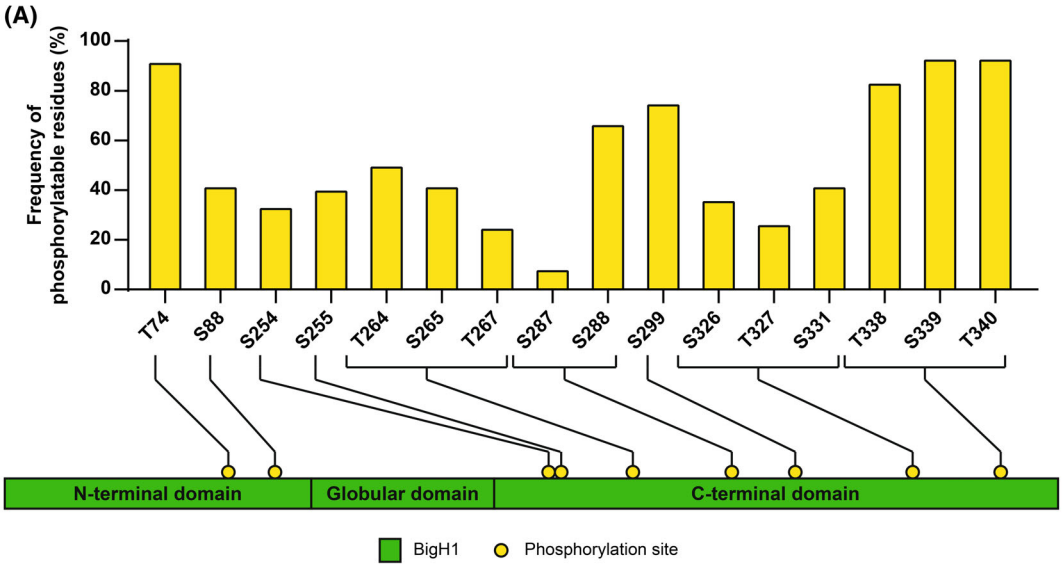
Among all identified phosphosites, peptides containing S265 showed the highest phosphorylation frequency (Table 1), suggesting that this is the most frequently phosphorylated amino acid in BigH1. The evaluation of the occupancy of the identified residues across orthologous sequences can elucidate additional potentially significant phosphorylation sites. To investigate this, we aligned 12 *Drosophila* BigH1 sequences and determined the frequency of phosphorylatable amino acids at each position of interest. Due to potential discrepancies in the alignments caused by variability in the N- and C-terminal regions of BigH1 orthologues, we used a consensus approach involving several alignment algorithms. Among the candidate sites, residues T74 and S339/T340 exhibited the highest values in sequence alignments, appearing in over 90% of the examined sequences (Fig. 1A, Table S1, Fig. S2).

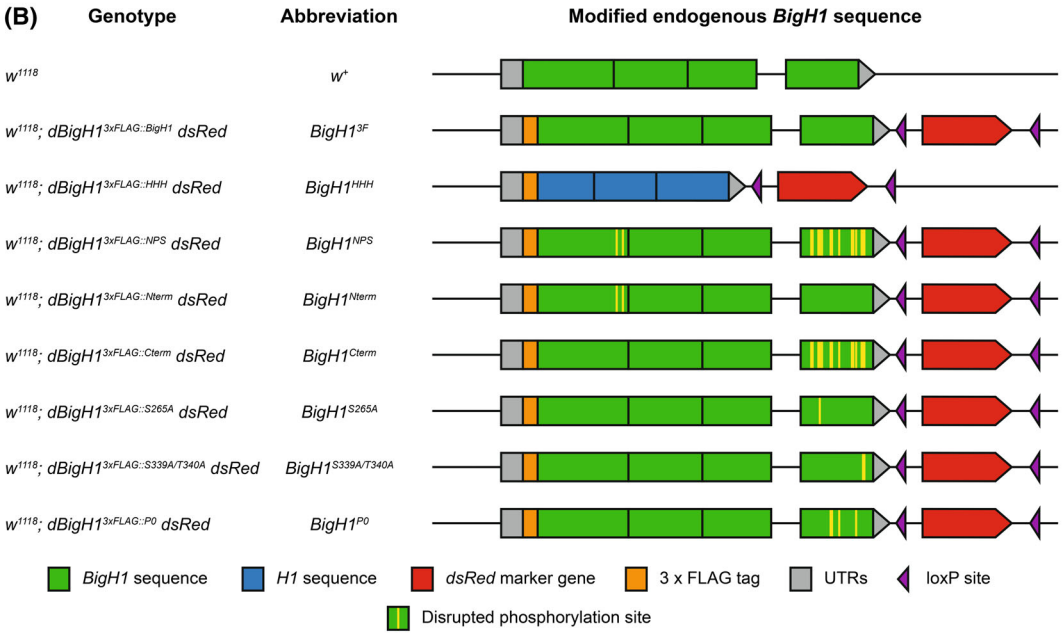
To address the importance of BigH1 phosphorylation, we created mutant *Drosophila* lines by modifying the endogenous *BigH1* sequence with CRISPR-Cas9 mutagenesis. Due to the complexity of the phosphorylation patterns and ambiguities in site localization in some cases (e.g., peptides containing S254/S255/T264/S265 or S326/T327/S331 residues), we adopted a conservative strategy and generated mutations of all potentially phosphorylated residues identified in the MS analysis. This approach ensured that no relevant modification site was overlooked, even if some sites (e.g., S265) are more consistently supported than others (Table 1). In these mutants, the affected serine- and threonine-coding sequences are either entirely or partially substituted by alanine-coding sequences. In $BigH1^{NPS}$ (NPS: no phosphorylation sites), all the putative serine and threonine residues are substituted by alanine, while $BigH1^{Nterm}$ and $BigH1^{Cterm}$ mutants only carry disrupted phosphorylation sites of either the N-, or the CTDs, respectively (Fig. 1B). Considering the proteomics results, conservation rates, and published data, we created further lines with point mutations carrying only one or a few disrupted phosphorylation sites to address their specific importances. In the $BigH1^{S265A}$ mutant, we mutated the phosphorylation site identified most frequently in the MS analysis. In the $BigH1^{S339A/T340A}$ mutant, phosphorylation sites with the highest frequency values by the alignment methods were substituted within the CTD, while the $BigH1^{P0}$ contains mutated residues previously identified as phosphorylation sites (S287/S288, S299 and S331) [24] (Fig. 1B). As controls, we used w^{1118}, and a *Drosophila* line expressing wild-type BigH1 with 3x FLAG epitope extension at the NTD ($BigH1^{3F}$). The 3x FLAG tag at the NTD does not affect BigH1 protein function as described previously [12]. Furthermore, as a positive control, we used a mutant *Drosophila* line in which the endogenous *BigH1*-coding sequence was entirely replaced by *H1*-coding sequence; hence, no functional BigH1 protein is present in these animals ($BigH1^{HHH}$) [12] (Fig. 1B). All the homozygous CRISPR-Cas9-edited alleles described above are viable and fertile under standard laboratory conditions (data not shown).

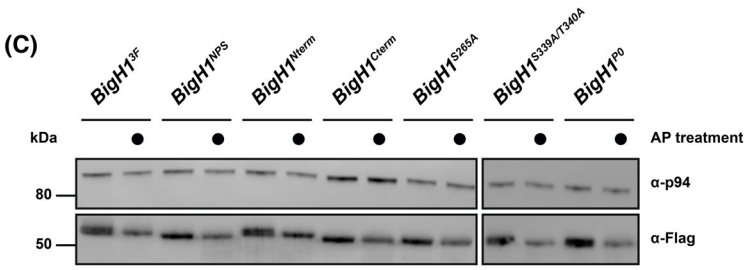
To confirm that 3× FLAG-tagged BigH1 proteins are expressed from the genetically modified alleles in early embryos, we performed western blot experiments using an anti-FLAG antibody. We found that each allele expresses a protein detectable with the antibody thereby confirming the presence of the modifications. In the case of the control ($BigH1^{3F}$), $BigH1^{Nterm}$, $BigH1^{S339A/T340A}$ and $BigH1^{P0}$ mutants, two separate bands were visible on the membrane (Fig. 1C). The slow-migrating isoform showed sensitivity to phosphatase treatment, confirming that these bands correspond to phosphorylated BigH1 proteins. The absence of the slow-migrating BigH1 isoform in $BigH1^{S265A}$, $BigH1^{Cterm}$, and $BigH1^{NPS}$ (where S265 is also mutated) samples identifies S265 as the primary target for phosphorylation on BigH1 (Fig. 1C). This result is consistent with the findings of the MS–MS proteomics experiment, where phosphorylation was more frequently observed on peptides containing the S265 residue (Table 1).

© 2026 The Author(s). *The FEBS Journal* published by John Wiley & Sons Ltd on behalf of Federation of European Biochemical Societies.

17424658, 0, Downloaded from https://febs.onlinelibrary.wiley.com/doi/10.1111/febs.70715 by HUN-REN Biological Research Center, Szeged, Wiley Online Library on [26/11/2026]. See the Terms and Conditions (https://onlinelibrary.wiley.com/terms-and-conditions) on Wiley Online Library for rules of use; OA articles are governed by the applicable Creative Commons License







© 2026 The Author(s). *The FEBS Journal* published by John Wiley & Sons Ltd on behalf of Federation of European Biochemical Societies.

17424658, 0, Downloaded from https://febs.onlinelibrary.wiley.com/doi/10.1111/febs.70715 by HUN-REN Biological Research Center, Szeged, Wiley Online Library on [26/11/2025]. See the Terms and Conditions (https://onlinelibrary.wiley.com/terms-and-conditions) on Wiley Online Library for rules of use; OA articles are governed by the applicable Creative Commons License

Fig. 1. Identification and biochemical validation of BigH1 phosphorylation sites using CRISPR-generated mutants. (A) Distribution of potential phosphorylation sites in BigH1. The y-axis shows the frequency of phosphorylatable residues (Ser and Thr) identified at specific amino acid positions within 12 *Drosophila* orthologues using multiple sequence alignment algorithms (MAFFT, T-coffee, Probcons, MUSCLE and MSAprobs) across 12 *Drosophila* species. Numbering corresponds to the *D. melanogaster* BigH1 reference. (B) Genomic map of the endogenous *BigH1* locus illustrating the positions of introduced mutations. The modifications include a *3xP3-dsRed* selection marker and were generated via CRISPR/Cas9-mediated gene editing. (C) Representative result of western blot analysis of early [0–2 h after egg laying (AEL)] wild-type and mutant embryos ($n = 2$). The presence of BigH1 and its phosphorylated forms were detected using an anti-FLAG antibody. The identity of the slow-migrating band as phosphorylated BigH1 was confirmed by its sensitivity to alkaline phosphatase (AP) treatment (lanes marked with black dots). Anti-p94 was used as a loading control.

Table 1. Phosphorylation sites identified in BigH1 by LC–MS–MS. For each phosphosite, the corresponding peptide sequence, the maximum Protein Prospector score observed across all datasets, the number of phosphopeptide spectra detected in 10 independent experiments, and the number of spectra corresponding to the unmodified peptide are shown. The 'max Score' column indicates the highest Protein Prospector peptide score obtained for the corresponding phosphopeptide across all analyzed datasets.

protein mods	DB peptide	Max score	Number of detected spectra in 10 experiments	Number of unphosphorylated spectra in 10 experiments
T74	NPYPTPPPDDGSK	29	16	69
S88	LVPPDSDNPK	25.2	9	98
S254|S255|T264|S265	AASSAAAQAMLETSQTAIPEAGK	54.2	226	204
S299	SIGTLAQPK	36.5	7	65
S326|T327|S331	GASTPDLSIMEAQATSTPQGATK	56.6	97	185
T339|S340	GASTPDLSIMEAQATSTPQGATK	41.7	5	185

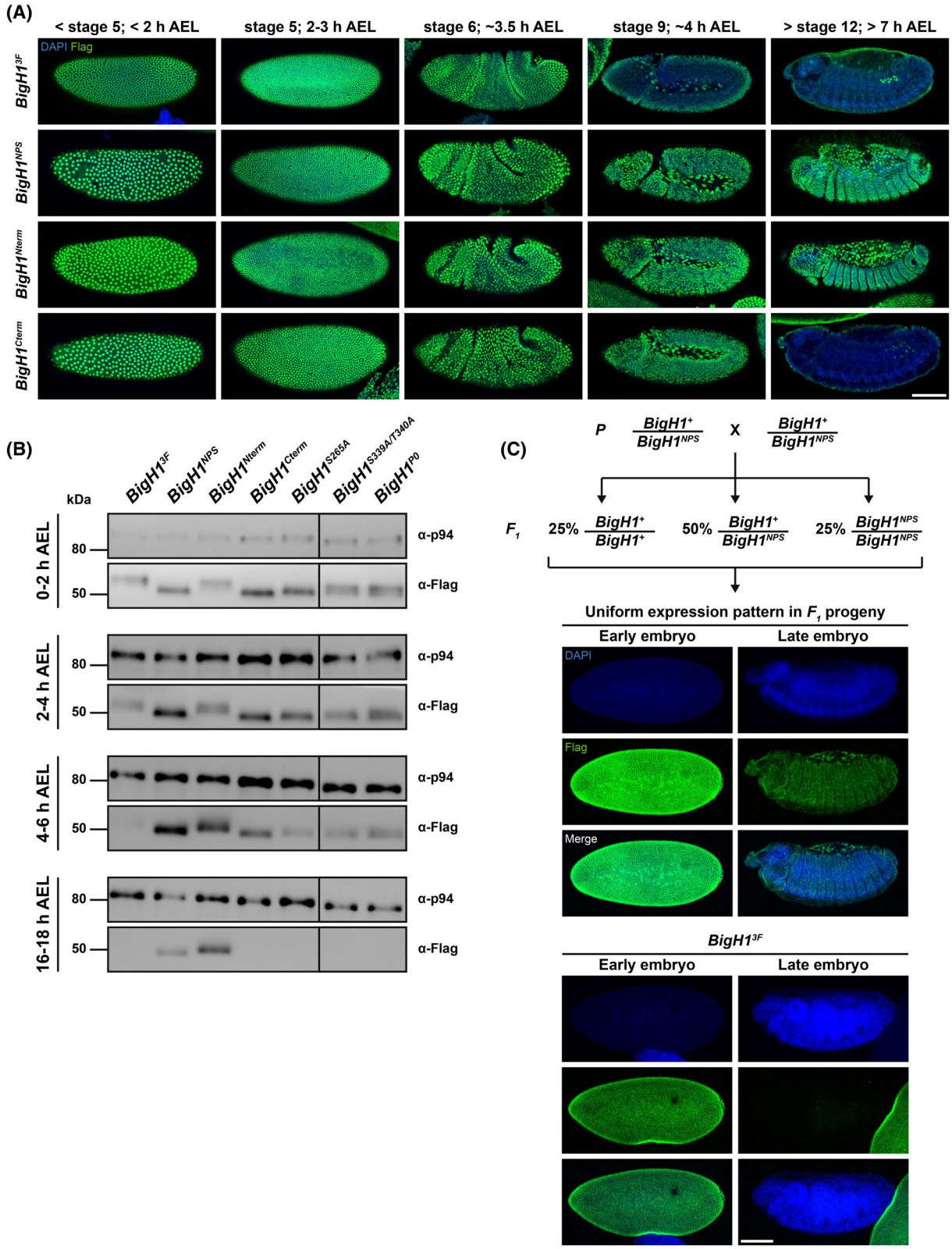
N-terminal phosphorylation is essential for maintaining proper expression pattern

Next, we assessed the temporal expression pattern of the different *BigH1* alleles in *Drosophila* embryos by immunohistochemistry and western blot experiments. During gastrulation [after developmental Stage 6 or ~ 3.5 h after egg laying (AEL)], wild-type BigH1 dissociates from the chromatin of somatic cells and is replaced by H1, as observed in control embryos expressing wild-type 3× FLAG-tagged BigH1 ($BigH1^{3F}$) (Fig. 2A,B), and consistent with previous reports [6,12]. Immunostaining experiments revealed that during the early stages of embryogenesis, all the modified protein alleles are present in the nuclei of mutant embryos visualized by anti-FLAG (Fig. 2A) or anti-BigH1 antibodies (Fig. S3). The presence of different BigH1 proteins during early development was also confirmed by western blot, as a clear FLAG signal was observed on the membrane in every case (Fig. 2B: 0–2 and 2–4 h AEL). Disruption of all phosphorylation sites on BigH1 led to its ectopic expression during later stages of development, as $BigH1^{NPS}$ displayed a prolonged presence of the protein observed in late-stage embryos (>developmental stage 10 or >5 h AEL) shown by FLAG- or BigH1-immunostaining (Fig. 2A, Fig. S3). This result was also confirmed by western blot, using protein extracts prepared from 16- to 18-h-old (developmental stage 17) embryos (Fig. 2B). Furthermore, we demonstrated that this temporal ectopic expression is primarily linked to the lack of NTD phosphorylation, as we observed similar phenotypes in the $BigH1^{Nterm}$ mutant (Fig. 2A,B, Fig. S3). The disruption of C-terminal phosphorylation does not lead to a similar phenotype, as the $BigH1^{Cterm}$ mutant does not show a sustained expression pattern observed in late embryos (similarly to $BigH1^{S265A}$, $BigH1^{S339A/T340A}$, and $BigH1^{P0}$ mutants) (Fig. 2B, Fig. S3). However, a slightly prolonged presence of $BigH1^{Cterm}$ can also be detected in the nuclei of somatic cells using FLAG antibody, as the protein is still visible after gastrulation in the nuclei of somatic cells, as observed in 4–6-h-old embryos validated by both immunofluorescence and western blot techniques (Fig. 2A,B). Similarly, $BigH1^{S265A}$, $BigH1^{S339A/T340A}$, and $BigH1^{P0}$ mutants also show a gradual decline in protein abundance as embryonic development progresses over time (Fig. 2B, Fig. S3).

In early Drosophila embryos, the protein and RNA products present before ZGA are largely maternally supplied during oogenesis. After fertilization, the paternal genome remains silent until ZGA, but maternally deposited gene products may persist even in the late stages of embryogenesis following ZGA [25,26]. Therefore, the prolonged presence of FLAG-$BigH1^{NPS}$ protein in late embryos could either reflect persistence of maternally deposited mutant protein or,

© 2026 The Author(s). *The FEBS Journal* published by John Wiley & Sons Ltd on behalf of Federation of European Biochemical Societies.

17424658, 0, Downloaded from https://febs.onlinelibrary.wiley.com/doi/10.1111/febs.70715 by HUN-REN Biological Research Center, Szeged, Wiley Online Library on [26/11/2026]. See the Terms and Conditions (https://onlinelibrary.wiley.com/terms-and-conditions) on Wiley Online Library for rules of use; OA articles are governed by the applicable Creative Commons License



© 2026 The Author(s). *The FEBS Journal* published by John Wiley & Sons Ltd on behalf of Federation of European Biochemical Societies.

17424658, 0, Downloaded from https://febs.onlinelibrary.wiley.com/doi/10.1111/febs.70715 by HUN-REN Biological Research Center, Szeged, Wiley Online Library on [26/11/2025]. See the Terms and Conditions (https://onlinelibrary.wiley.com/terms-and-conditions) on Wiley Online Library for rules of use; OA articles are governed by the applicable Creative Commons License

Fig. 2. Spatiotemporal expression pattern of wild-type and mutant BigH1 during embryogenesis. (A) Immunostaining shows the representative distribution of wild-type and mutant BigH1 proteins at indicated embryonic stages based on at least three biological replicates per genotype and developmental stage. BigH1 localization was detected using an anti-Flag antibody (green); DNA was stained with DAPI (blue). Scale bar represents 100 μm. (B) Representative western blot analysis demonstrates the presence of BigH1 in wild-type and mutant embryos during embryogenesis ($n = 5$). Protein extracts were prepared from embryos aging 0–2 h, 2–4 h, 4–6 h, and 16–18 h after egg laying (AEL). Anti-p94 was used as a loading control. (C) Representative confocal images show *F1* embryos derived from $BigH1^{NPS}$ heterozygous parents during early (≤ Stage 5; ≤3 h AEL) and late (>Stage 12; >7 h AEL) embryogenesis. Despite genotypic variance within the F_1 population, 100% of late embryos (>Stage 12; >7 h AEL; $N = 267$) exhibit a uniform ectopic expression pattern. Control ($BigH1^{3F}$) embryos ($N = 13$) do not exhibit prolonged persistence of BigH1 at the same stage of development. BigH1 was stained with anti-Flag (green), and nuclei were visualized with DAPI (blue). Scale bar represents 100 μm.

alternatively, zygotic expression of the mutant allele after ZGA.

In order to determine whether the abnormally persistent protein originated from the mother or was the result of zygotic expression, we crossed $BigH1^{NPS}/BigH1^{+}$ heterozygous females and males. In this cross, all embryos develop from mothers depositing FLAG-tagged BigH1^{NPS} protein during oogenesis, whereas Mendelian inheritance predicts that only 75% of the embryos inherit the $BigH1^{NPS}$ allele zygotically and 25% are homozygous wild-type. Embryos were not individually genotyped; however, if the persistent FLAG signal depended on zygotic expression of $BigH1^{NPS}$, approximately 25% of the embryos should be lacking FLAG-BigH1^{NPS} at the late stages of embryogenesis.

Using FLAG-immunostaining, we found that in 100% of embryos derived from the cross ($n = 252$) BigH1^{NPS} persists until late embryogenesis (>6 h AEL). In contrast, $BigH1^{3F}$ control embryos do not show a sustained presence of BigH1 in the nuclei of their somatic cells at this stage of development ($n = 13$) (Fig. 2C). These data indicate that the prolonged FLAG-BigH1^{NPS} signal is best explained by the persistence of the maternally deposited mutant protein rather than by its zygotic expression after ZGA. Moreover, because FLAG-BigH1^{NPS} persists despite the presence of wild-type BigH1 protein in heterozygous embryos, whereas FLAG-tagged wild-type BigH1 does not, the nonphosphorylatable mutant protein behaves dominantly with respect to the prolonged embryonic persistence.

The above results raised the question of how loss of BigH1 phosphorylation contributes to its abnormal persistence during embryogenesis. One possibility is that the nonphosphorylatable BigH1^{NPS} protein has an increased half-life. Alternatively, persistent BigH1 protein could, at least in principle, result from sustained BigH1 mRNA abundance and continued translation at later embryonic stages. To test whether BigH1 persistence is associated with altered *BigH1* mRNA levels when phosphorylation sites are mutated, we measured *BigH1* transcript abundance by RT-qPCR in 0–2 h-, 4–6 h-, and 16–18-h-old embryos produced by females heterozygous for the CRISPR-Cas9-modified alleles $BigH1^{3F}$, $BigH1^{Nterm}$, $BigH1^{Cterm}$, or $BigH1^{NPS}$, each crossed to wild-type w^{1118} males. Embryos from each cross were analyzed as bulk, ungenotyped populations. To distinguish transcripts produced from the modified and unmodified alleles, we used primer sets specific for either the FLAG-coding sequence or the untagged wild-type *BigH1* coding sequence.

In the embryos derived from $BigH1^{Nterm}/BigH1^{+}$ females, both FLAG-tagged and untagged *BigH1* mRNA levels declined over developmental time with kinetics similar to those observed in the embryos of the $BigH1^{3F}/BigH1^{+}$ control females (Fig. S4A,B). Thus, the loss of N-terminal phosphorylation alone is not associated with increased *BigH1* mRNA abundance. *BigH1* mRNA levels also decreased over time in embryos derived from $BigH1^{Cterm}/BigH1^{+}$ and $BigH1^{NPS}/BigH1^{+}$ females. However, in the embryos of these females, the decline was less pronounced, and higher *BigH1* mRNA levels were detected at later developmental stages, particularly at 4–6 and 16–18 h AEL, compared with those of the $BigH1^{3F}$ and $BigH1^{Nterm}$ heterozygous females (Fig. S4A,B). Because the FLAG-tagged and untagged BigH1 transcripts were affected similarly within each maternal genotype, these changes do not support the selective stabilization of the mutant mRNA. Instead, they reveal that the C-terminal mutations, present in both $BigH1^{Cterm}$ and $BigH1^{NPS}$, are associated with a genotype-dependent increase in overall *BigH1* mRNA abundance at later embryonic stages.

Together, these data indicate that the abnormal persistence of $BigH1^{NPS}$ is unlikely to be explained by allele-specific stabilization of the mutant transcript. Rather, the prolonged presence of BigH1^{NPS} protein is more consistent with increased stability of the mutant

© 2026 The Author(s). *The FEBS Journal* published by John Wiley & Sons Ltd on behalf of Federation of European Biochemical Societies.

17424658, 0, Downloaded from https://febs.onlinelibrary.wiley.com/doi/10.1111/febs.70715 by HUN-REN Biological Research Center, Szeged, Wiley Online Library on [26/11/2026]. See the Terms and Conditions (https://onlinelibrary.wiley.com/terms-and-conditions) on Wiley Online Library for rules of use; OA articles are governed by the applicable Creative Commons License

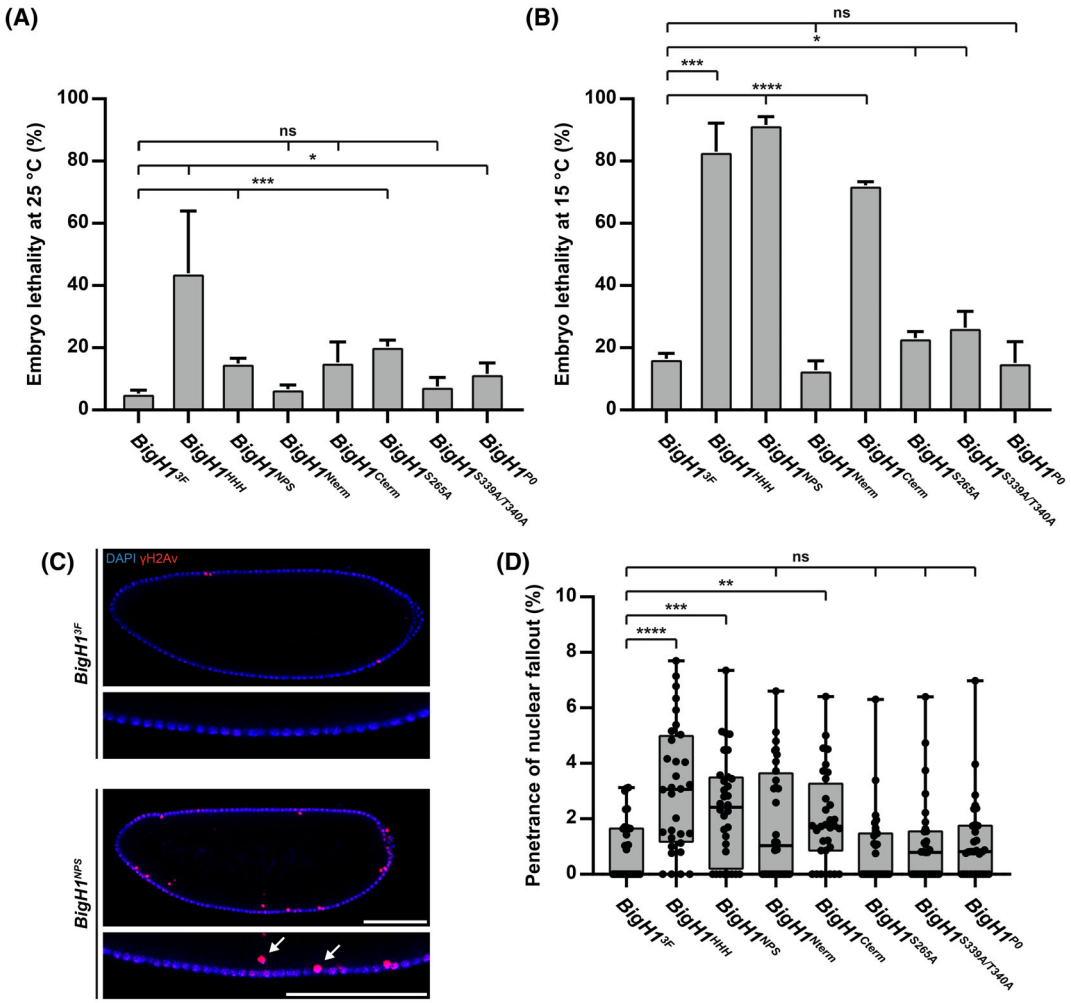


Fig. 3. Disruption of BigH1 phosphorylation sites impairs early embryonic development and viability. Lethality rates of mutant embryos at 25 °C (A) and at 15 °C (B). Bars are based on the mean, SD and sample number of total counted cases as follows: at 25 °C *BigH1*^{3F} (N = 834), *BigH1*^{HHH} (N = 390), *BigH1*^{NPS} (N = 747), *BigH1*^{Nterm} (N = 469), *BigH1*^{Cterm} (N = 796) *BigH1*^{S265A} (N = 504), *BigH1*$^{S339A/T340A}$ (N = 610), and *BigH1*^{P0} (N = 536); and at 15 °C: *BigH1*^{3F} (N = 773), *BigH1*^{HHH} (N = 209), *BigH1*^{NPS} (N = 429), *BigH1*^{Nterm} (N = 352), *BigH1*^{Cterm} (N = 574) *BigH1*^{S265A} (N = 1145), *BigH1*$^{S339A/T340A}$ (N = 600), and *BigH1*^{P0} (N = 639). For the statistics, mean values of three independent experiments were used to perform unpaired, two-tailed t-tests. *P*-values are represented as follows: ns (nonsignificant) $P \geq 0.05$; *$P < 0.05$; **$P < 0.01$; ***$P < 0.001$; ****$P < 0.0001$. (C) Confocal images demonstrate nuclear fallout in precellular embryos [0–3 h after egg laying (AEL)] of *BigH1*^{3F} and *BigH1*^{NPS} flies. γH2A staining (red) marks nuclei with compromised DNA integrity targeted for elimination. DAPI labels total DNA (blue) and white arrows indicate nuclei undergoing fallout. Scale bar represents 100 μm. (D) Penetrance of nuclear fallout of control (*BigH1*^{3F}) and mutant embryos. Boxplots: median (center line), 25th–75th percentiles (box), and min-max (whiskers). Individual points indicate the percentage of γH2A-positive nuclei quantified within a single lateral region of an embryo. Total lateral regions counted as follows: *BigH1*^{3F} (N = 31), *BigH1*^{HHH} (N = 32), *BigH1*^{NPS} (N = 32), *BigH1*^{Nterm} (N = 32), *BigH1*^{Cterm} (N = 32) *BigH1*^{S265A} (N = 31), *BigH1*$^{S339A/T340A}$ (N = 31), and *BigH1*^{P0} (N = 31). Statistical significance was determined using Mann–Whitney U-tests, as all group comparisons failed the normality assumption via the Shapiro–Wilk test. *P*-values are represented as follows: ns (nonsignificant) $P \geq 0.05$; *$P < 0.05$; **$P < 0.01$; ***$P < 0.001$; ****$P < 0.0001$.

protein. Although a contribution from altered overall *BigH1* mRNA abundance in embryos carrying C-terminal mutations cannot be fully excluded, this hypothesis is not supported by the observation that the BigH1^{Cterm} mutant protein, unlike BigH1^{NPS}, does not persist until the end of embryogenesis (Fig. 2A,B).

C-terminal phosphorylation is essential for proper embryonic development

It has previously been shown that the absence of BigH1 (replacement by H1) causes reduced embryo viability due to defects in precellular nuclear divisions,

© 2026 The Author(s). *The FEBS Journal* published by John Wiley & Sons Ltd on behalf of Federation of European Biochemical Societies.

17424658, 0, Downloaded from https://febs.onlinelibrary.wiley.com/doi/10.1111/febs.70715 by HUN-REN Biological Research Center, Szeged, Wiley Online Library on [26/11/2026]. See the Terms and Conditions (https://onlinelibrary.wiley.com/terms-and-conditions) on Wiley Online Library for rules of use; OA articles are governed by the applicable Creative Commons License

especially at suboptimal temperature (15 °C) [12]. Therefore, we investigated how impaired BigH1 phosphorylation impacts embryo viability. We found that, similarly to the replacement of BigH1 by H1, $BigH1^{NPS}$ mutant embryos exhibited slightly increased lethality at 25 °C (Fig. 3A), moreover, $BigH1^{NPS}$ and $BigH1^{Cterm}$ showed severe embryo lethality at 15 °C as compared to $BigH1^{3F}$ (Fig. 3B). The observed lethality strongly correlates with the elevated frequency of nuclear cleavage defects, as we observed increased incidence of nuclear fallout in both $BigH1^{NPS}$ and $BigH1^{Cterm}$ mutants (Fig. 3C,D). These results revealed that C terminus phosphorylation of BigH1 plays a crucial role in embryo viability, particularly under suboptimal conditions. Interestingly, $BigH1^{Nterm}$ mutant embryos do not show decreased viability at either 25 °C or 15 °C (Fig. 3A,B), despite the high penetrance of nuclear defects (Fig. 3D). This suggests that the high frequency of defective nuclei present in precellular embryos does not necessarily lead to embryonic lethality. Although we found that $BigH1^{S265A}$, $BigH1^{P0}$, and $BigH1^{S339A/T340A}$ mutant embryos exhibit moderate lethality at 25 °C and/or 15 °C, this difference is considerably lower than that observed in $BigH1^{NPS}$ and $BigH1^{Cterm}$ mutants at suboptimal temperatures (Fig. 3A,B). These results reveal that the CTD of BigH1 does not contain any single, functionally highly relevant phosphorylation site, but rather that these sites appear to be functionally redundant. Thus, we can conclude that CTD phosphorylation is generally required for proper embryonic development, but the specific positioning of these modifications appears to be interchangeable.

However, an additional consideration must be addressed here. Excessive amino acid substitutions may compromise the structural integrity of BigH1 and thus render the protein nonfunctional, leading to a similar phenotype [27]. As previously reported, the absence of BigH1 is compensated for by the induction of premature H1 expression during early embryogenesis [28,29]. Through this process, in contrast to the wild-type, somatic H1 becomes quantitatively enriched by the translation of maternal mRNA in early, *BigH1* mutant embryos, possibly contributing to their survival [27]. To examine whether linker histone compensation occurs in $BigH1^{NPS}$ mutant embryos, we performed immunostaining with H1 antibody. Our observations demonstrate that H1 levels in $BigH1^{NPS}$ mutants do not increase during early embryogenesis (≤developmental stage 5 or ≤3 h AEL) compared to $BigH1^{3F}$ control embryos, that is, H1 compensation did not occur (Fig. S5 left panel). This suggests that the protein remains functional despite the high number of mutations present in $BigH1^{NPS}$ flies. After the early stages of development, H1 levels increase in both genotypes as was demonstrated in embryos undergoing gastrulation (developmental stage 9 or ~ 4 h AEL) (Fig. S5, right panel).

Discussion

In this study, we demonstrate that BigH1 is subject to extensive phosphorylation at both its N- and CTDs in early *Drosophila* embryos, and the phosphorylation of these two domains exerts fundamentally distinct biological functions. Simultaneous mutation of the two major N-terminal phosphoacceptor sites (S74 and T88) leads to the persistence of BigH1 until the end of embryogenesis, in sharp contrast to the wild-type protein, which is eliminated during gastrulation. Our results suggest that this phenotype has a dominant maternal-effect component, as it appears in all offspring embryos even when the mother is heterozygous for the mutations. We further show that the disruption of N-terminal phosphorylation is not associated with increased BigH1 mRNA abundance in embryos, indicating that the persistence of the mutant protein is unlikely to be explained by elevated transcript levels. Histone proteins are characterized by a high degree of stability [30–32]. For example, the half-life of H1.2 in mouse B1 cells is 2242 h [33]. Therefore, during rapid developmental transitions that require large-scale chromatin reorganization and linker histone exchange, the degradation of the replaced H1 histones must be tightly regulated. Linker histone exchange is a hallmark of maternal-to-zygotic transition (MZT) and is thought to be necessary for the reprogramming of the nuclei from a transcriptionally inactive chromatin state regulated by maternally provided factors to a transcriptionally active state, allowing cell differentiation [5,34]. Our results suggest that NTD phosphorylation plays a crucial role in the regulated removal and/or degradation of BigH1, supporting BigH1-H1 replacement and MZT during early embryogenesis. Previous work has shown that BigH1 expression is also regulated at the mRNA level during embryogenesis, as BigH1 translation and mRNA stability are controlled by the brain tumor (Brat) protein [35]. Our results identify N-terminal phosphorylation as an additional regulatory mechanism that controls BigH1 persistence at the protein level during embryogenesis.

In contrast to the N-terminal mutants, the disruption of CTD phosphorylation does not affect BigH1 temporal expression but leads to defects in nuclear divisions accompanied by γH2Av accumulation and

© 2026 The Author(s). *The FEBS Journal* published by John Wiley & Sons Ltd on behalf of Federation of European Biochemical Societies.

17424658, 0, Downloaded from https://febs.onlinelibrary.wiley.com/doi/10.1111/febs.70715 by HUN-REN Biological Research Center, Szeged, Wiley Online Library on [26/11/2026]. See the Terms and Conditions (https://onlinelibrary.wiley.com/terms-and-conditions) on Wiley Online Library for rules of use; OA articles are governed by the applicable Creative Commons License

reduced embryonic viability, particularly at low temperature. These phenotypes are characteristics of replication stress in the syncytial embryo, where S phases last only a few minutes and chromatin assembly must keep pace with DNA synthesis [11,12]. Canonical H1 proteins in metazoans are known to undergo cell-cycle-regulated phosphorylation, which weakens their affinity for chromatin and facilitates mobilization during replication [36–39]. Since our results suggest that the absence of C-terminal phosphorylation causes errors in early syncytial divisions, CTD phosphorylation may facilitate rapid nucleosome disassembly during replication. By modulating the strength of the H1-nucleosome interaction, this modification could render DNA more accessible to the replication machinery. Mass spectrometry identified S265 as the most abundantly modified phosphorylation site at the CTD. This finding is further supported by the observation that, in the case of alleles carrying the S265A mutation ($BigH1^{S265A}$, $BigH1^{Cterm}$, and $BigH1^{NPS}$), no phosphatase-reactive slow-migrating band was detected in the western blot assay. Interestingly, this mutation of this single residue alone produces only mild phenotypes. Combinatorial mutants affecting other conserved phosphorylation sites were similarly tolerated. This suggests that CTD phosphorylation operates through cooperative or redundant modifications, a phenomenon well documented for linker histones and core histones alike [40,41]. Phosphorylation of multiple residues may collectively modulate BigH1 conformation or charge distribution, and thus, the disruption of any single site may be buffered by the remaining phosphosites.

Based on our results, we propose a model in which BigH1 phosphorylation coordinates two temporally and mechanistically distinct processes. During the syncytial divisions, CTD phosphorylation modulates BigH1–chromatin interactions to ensure the rapid replication process. Later, under MZT, NTD phosphorylation triggers BigH1 eviction and/or degradation, allowing somatic H1 to subsequently fill the role of the linker histone in the nuclei of somatic cells. This dual regulatory logic allows BigH1 to fulfill the unique requirements of early embryonic chromatin: exceptional dynamics during abbreviated cell cycles, followed by rapid clearance when it is no longer needed. Future work aimed at identifying the responsible kinases and defining the structural consequences of BigH1 phosphorylation will be essential to better elucidate how this embryonic linker histone orchestrates chromatin dynamics at the onset of life.

Materials and methods

Identification of phosphorylation sites and their occupancies in orthologues

To identify BigH1 phosphorylation sites in *Drosophila* embryos, freshly collected embryos were frozen 1–2 h AEL (syncytial blastoderm stage, Stages 2–3) in liquid nitrogen and ground using a TissueLyser (50 Hz, 2 min). Total proteins were extracted with the manufacturer's lysis buffer supplemented with 1 mM DTT, 1 mM PMSF, 1× protease inhibitor cocktail (cat. no.: 78438; Thermo Fisher Scientific™, Waltham, MA, USA), and 1× phosphatase inhibitor cocktail (cat. no.: 04906845001; PhosSTOP™, Roche, Basel, Switzerland). Protein extracts (2–3 mg per IP) were immunopurified using anti-FLAG antibody coupled to 50 nm magnetic beads (cat. no.: 130-101-591; MACS® Technology, Miltenyi, Bergisch Gladbach, Germany), following a protocol modified from [42]. Bound proteins were reduced with 10 mM DTT, alkylated with 22 mM IAM, and digested on-column with sequencing-grade trypsin (cat. no.: V5111; Promega, Madison, WI, USA). Ten independent IPs were used for the analyses.

The digestion mixtures were acidified and transferred to single-use trapping mini-columns (Evotip; 1/8 of each sample), then analyzed by LC–MS–MS using an Evosep One system (LC: 15 SPD; MS1 resolution: 120 000) online coupled to an Orbitrap Fusion Lumos mass spectrometer (Thermo Fisher Scientific) operating in positive ion mode. Data acquisition was performed in data-dependent mode, with multiply charged ions selected from each MS survey scan for ion-trap HCD fragmentation. MS spectra were acquired in the Orbitrap (resolution = 60 000), while MS–MS spectra were recorded in the ion trap.

Raw data were converted into peak lists using Proteome Discoverer (v1.4) and searched against the SwissProt database (downloaded 2022/06/12; 570 252 proteins) using the Protein Prospector search engine (v5.15.1). Search parameters were as follows: enzyme, trypsin (maximum two missed cleavages); precursor mass tolerance, 5 ppm; fragment mass tolerance, 10 ppm (both monoisotopic); fixed modification, carbamidomethylation of cysteine residues; variable modifications, acetylation of protein N-termini, methionine oxidation, cyclization of N-terminal glutamine residues, and phosphorylation of Ser, Thr, and Tyr residues. Acceptance criteria: minimum scores of 22 (proteins) and 20 (peptides); maximum E values of 0.01 and 0.05 for protein and peptide identifications, respectively. The quality of individual MS–MS spectra was characterized by the spectrum score calculated by Protein Prospector, which reflects the degree of agreement between the measured fragment ion pattern and the theoretical fragmentation of the assigned peptide. For each peptide, the highest-scoring (best-matching) spectrum was reported as the maximum spectrum score.

© 2026 The Author(s). *The FEBS Journal* published by John Wiley & Sons Ltd on behalf of Federation of European Biochemical Societies.

17424658, 0, Downloaded from https://febs.onlinelibrary.wiley.com/doi/10.1111/febs.70715 by HUN-REN Biological Research Center, Szeged, Wiley Online Library on [26/11/2026]. See the Terms and Conditions (https://onlinelibrary.wiley.com/terms-and-conditions) on Wiley Online Library for rules of use; OA articles are governed by the applicable Creative Commons License

To address the occupancy of the identified phosphosites in orthologues, we aligned BigH1 sequences of 12 *Drosophila* species using the Jalview software. Alignments were made by MAFFT, T-coffee, Probcons, MUSCLE, and MSAprobs algorithms with standard settings [43]. Threonine–serine differences of a given site were considered as a match in every case. For representative alignment, the MAFFT method was performed.

Establishment of mutant *Drosophila* lines

For the generation of *BigH1* mutant *Drosophila* lines, we used CRISPR-Cas9 genome editing [44]. Donor plasmids carrying mutated *BigH1* sequences were injected into embryos expressing Cas9 and *BigH1*-specific gRNAs (as described in [12]). This setup was designed to facilitate homology-directed repair, effectively replacing the endogenous wild-type *BigH1* locus with mutated ones. Donor plasmids contain homology arms, a P3 promoter-driven *dsRed* marker gene, and mutated BigH1 sequences generated from the donor plasmid described in [12]. $BigH1^{NPS}$ sequence was created by gene synthesis (Eurofins Genomics); meanwhile, $BigH1^{Cterm}$ and $BigH1^{Nterm}$ sequences were generated using combinations of BstXI-digested fragments of the wild-type and $BigH1^{NPS}$ sequences in the pUC18 subclone (carrying the *BstZ17I-BglII* fragment of the donor plasmid). Other *BigH1* mutant sequences were created by site-directed mutagenesis and Sequence and Ligation Independent Cloning (SLIC) methods [45] on the *BigH1* subclone. Establishment of *BigH1* mutant *Drosophila* lines was carried out as described in [12].

Protein extract preparation for western blotting

Embryos were collected at 0–2 h, 2–4 h, 4–6 h and 16–17 h AEL, frozen in liquid nitrogen, and stored at −80 °C until sample preparation. Frozen embryos were smashed with plastic pestle in different lysis buffers depending on the experiment, and were kept on ice during the whole procedure. For the alkalic phosphatase treatment, detergent-free RIPA buffer (25 mM Tris–HCl pH = 7.5; 150.4 mM NaCl; 0.5% Na-deoxycholate) supplemented with 1x Protease Inhibitor Cocktail, FastAP buffer and 1 U FastAP (cat. no.: EF0654; Thermo Fisher Scientific) was applied. Phosphatase treatment was done at 37 °C for 10 min. Control samples also contained FastAP buffer, but not the enzyme and were kept on ice during the whole time. For demonstrating temporal expression patterns, Laemmli buffer (50 mM Tris–HCl pH = 6.8; 10% glycerol; 5% β-Mercaptoethanol; 20 $g{\cdot}L^{-1}$ SDS; 0.5 $g{\cdot}L^{-1}$ Bromophenol Blue) supplemented with 0.5 μM okadaic acid and 1× PhosSTOP reagent was used. Samples were stored on ice for 30 min after homogenization and then centrifuged (12 000 ***g*** for 10 min at 4 °C). Supernatant was boiled at 100 °C for 5 min then loaded on gels. Samples without denaturing agent were supplemented with loading buffer prior to boiling.

Western blotting

To resolve the slow-migrating phosphorylated BigH1 isoforms, proteins were separated using a 4–12% Bis-Tris NuPAGE® gel system (cat. no.: NP0323BOX; Invitrogen, Thermo Fisher Scientific) according to the manufacturer's protocol for both the running and transfer steps using a nitrocellulose membrane. To investigate the changes in protein levels during the different stages of embryogenesis, SDS/PAGE system-based western blot experiments were performed. Proteins were separated on 12% SDS-polyacrylamide gels. (Running gel: 373.3 mM Tris–HCl pH = 8.8; 12% Acrylamide/bis-acrylamide (29:1); 0.1% SDS; 0.08467% APS; 0.0867% TEMED. Stacking gel: 83.3 mM Tris–HCl pH = 6.8; 3.333% Acrylamide/bis-acrylamide (29:1); 0.067% SDS; 0.067% APS; 0.06% TEMED.) Gels were run in SDS/PAGE buffer (25 mM Tris–HCl pH = 8.3; 192 mM glycine; 1% SDS). Samples were transferred to nitrocellulose membrane in transfer buffer (25 mM Tris–HCl pH = 8.3; 192 mM glycine; 10% methanol) overnight at 4 °C. Following Ponceau's staining and blocking steps with 5% milk powder in TBS-Tween for 1 h, primary antibodies were applied overnight at 4 °C. After washing with TBS-Tween for 4 × 10 min, samples were incubated in secondary antibodies at room temperature for 2 h. Following washing steps of TBS-Tween for 4 × 10 min, SuperSignal™ West Pico PLUS Chemiluminescent Substrate (cat. no.: 34580; Thermo Fisher Scientific) was applied before detecting the chemiluminescent signal with a Uvitech Alliance Q9 Advanced imaging platform. Utilized antibodies are shown in Table 2.

Viability tests

To investigate embryo viabilities, flies were kept at 25 °C to lay eggs. Embryos were collected at 0–30 min AEL and placed at 25 °C or at 15 °C until hatching. Lethality rates were determined by analyzing the hatching rates after 36 or 96 h of incubation, respectively. For the statistics, mean values of three independent experiments were used to perform unpaired, two-tailed *t*-tests.

Immunohistochemistry and microscopy

Embryos were dechorionated with bleach (3% NaClO), fixed in a 1:1 mixture of heptane:PBS and 4% formaldehyde for 20 min, devitellinized with shaking in a 1:1 heptane:methanol, then stored in methanol at −20 °C. Samples were rehydrated by washing with 2:1, 1:1, and 1:2 mixtures of methanol:PBT (0.1% Triton X-100 in PBS) for 5 min,

© 2026 The Author(s). *The FEBS Journal* published by John Wiley & Sons Ltd on behalf of Federation of European Biochemical Societies.

17424658, 0, Downloaded from https://febs.onlinelibrary.wiley.com/doi/10.1111/febs.70715 by HUN-REN Biological Research Center, Szeged, Wiley Online Library on [26/11/2026]. See the Terms and Conditions (https://onlinelibrary.wiley.com/terms-and-conditions) on Wiley Online Library for rules of use; OA articles are governed by the applicable Creative Commons License

Table 2. List of antibodies and stains used in western blot (WB) and immunohistochemistry (IHC) experiments.

Primary antibodies	Dilution	Source	Application
α-FLAG M2	1:1000 1:5000	Sigma (F1804)	IHC, WB
α-BigH1	1:600	Fernando Azorín described in [6]	IHC
α-dH1	1:3000	James T. Kadonaga described in [47]	IHC
α-γH2Av	1:1000	DSHB (UNC93-5.2.1)	IHC
α-p94	1:1000	Andor Udvardy described in [48]	WB
α-H3	1:5000	Abcam (AB1791)	WB
Secondary antibodies and DAPI			
α-mouse, HRP conjugated	1:5000	Invitrogen (A16066)	WB
α-rabbit, HRP conjugated	1:5000	Invitrogen (G-21234)	WB
α-mouse, Alexa Fluor 488 conjugated	1:600	Invitrogen (A11001)	IHC
α-rat, Alexa Fluor 647 conjugated	1:600	Thermo Fisher Scientific (A-21247)	IHC
α-rabbit, Alexa Fluor 555 conjugated	1:600	Thermo Fisher Scientific (A-21428)	IHC
DAPI	300 nM	Sigma (D9542)	IHC

washed with PBT for 3 × 5 min then blocked in PBT-N (0.1% Triton X-100, 1% BSA, 5% FCS in PBS) for 1 h. Primary antibodies were applied overnight at 4 °C. Samples were washed with PBT for 3 × 10 min, then secondary antibodies were used at room temperature for 1 h, meanwhile samples were protected from light. Following washing steps with PBT for 3 × 10 min, embryos were mounted in Fluoromount-G (cat. no.: 00-4958-02; Invitrogen, Thermo Fisher Scientific) on microscope slides. Antibodies used in the immunohistochemistry are shown in Table 2.

Confocal images were acquired using a Zeiss LSM 800 microscope equipped with a Plan-Apochromat 20×/0.8 M27 objective and a spinning disk confocal microscope (Visitron Spinning Disk Confocal System with Yokogawa CSU-W1 unit and Andor Zyla 4.2 PLUS sCMOS camera) using 10x dry (NA: 0.3) and 20× dry (NA: 0.45) objectives. For image processing and visualization, the Fiji software version [46] was used. To statistically analyze the penetrance of the nuclear fallout phenotype, Mann–Whitney U-tests were performed, as all group comparisons failed the normality assumption via the Shapiro–Wilk test.

Real-time quantitative PCR

Twenty to thirty milligrams of frozen embryos were homogenized in 800 µL of TRIzol (cat. no.: 15 596 018; Invitrogen, Thermo Fisher Scientific) and centrifuged at 12 000 ***g*** for 10 min at 4 °C. Two hundred microliters of chloroform was added to the cleared supernatant, shaken, and incubated for 2–3 min at RT. Mixtures were centrifuged at 12 000 ***g*** for 15 min at 4 °C. Aqueous phases were removed and mixed with 500 µL isopropanol, incubated for 10 min at RT, and centrifuged at 12 000 *g* for 10 min at 4 °C. RNA pellets were washed with 75% ethanol, vacuum dried, and resuspended in RNase-free water. RNA samples were treated with DNase I (cat. no.: EN0521; Thermo Fisher Scientific) according to the manufacturer's protocol. DNase I-digested RNA samples were extracted by 0.1 volume of 5 M ammonium acetate and 1 volume of isopropanol, washed with 75% ethanol, vacuum dried, and resuspended in RNase-free water. One microliter of RNA was used for cDNA synthesis made by RevertAid First Strand cDNA Synthesis Kit (cat. no.: K1622; Thermo Fisher Scientific) according to the manufacturer's protocol. We performed the qPCR reaction using a 20-fold cDNA dilution as the template, with 2× Universal SYBR Green Fast qPCR mix (cat. no.: RK21203; ABclonal, Woburn, MA, USA), on a Rotor-Gene Q instrument (Qiagen, Hilden, Germany). For data analysis, the Qiagen Rotor-Gene Q software was used. Relative gene expression of BigH1 was measured by RT-qPCR quantification using the $2^{-\Delta\Delta Ct}$ method and normalized to *RpL13A* gene based on three biological and two to three technical replicates for each condition. To measure the expression of CRISPR-edited alleles, we used a pair of primers specific to the Flag sequence, while to measure the expression of wild-type BigH1, we used a pair of primers specific to the unedited BigH1 sequence. Primers used in the RT-qPCR experiment are shown in Table 3. For statistical analysis, mixed-effects

Table 3. Primers used in RT-qPCR experiment.

Primer name	5′-3′ sequence	Target
Flag Fw	CTACAAAGACCATGACGGTG	CRISPR-Cas9 modified *BigH1* alleles
qBigH1 Rev3	CATATTGGAGTCTTCGGATTCG	
qBigH1 Fw4	CAATTTAATTTCCAACTAATAACATGG	Wild-type (unmodified) *BigH1* allele
qBigH1 Rev4	CTCTTCTTCGCCCATATTGG	
RpI13A Fw	GTGGTGGCCAAGTACCTGTT	*RpL13A* (housekeeping gene)
RpI13A Rev	GTGGGATCATGCCTCGGACT	

© 2026 The Author(s). *The FEBS Journal* published by John Wiley & Sons Ltd on behalf of Federation of European Biochemical Societies.

17424658, 0, Downloaded from https://febs.onlinelibrary.wiley.com/doi/10.1111/febs.70715 by HUN-REN Biological Research Center, Szeged, Wiley Online Library on [26/11/2026]. See the Terms and Conditions (https://onlinelibrary.wiley.com/terms-and-conditions) on Wiley Online Library for rules of use; OA articles are governed by the applicable Creative Commons License

model restricted maximum likelihood (REML) was conducted followed by Tukey's post hoc test.

Acknowledgements

This work was supported by the National Research Development and Innovation Office (K143248 and K151375 to GT and OTKA-142961 to BG and ZV), the National Laboratory for Biotechnology program (2022-2.1.1-NL-2022-00008 to PV), and the EU's Horizon 2020 research and innovation program under grant agreement (no.: 739593 to AP). We thank Katalin Ökrösné for her technical assistance, Fernando Azorín for the α-dBigH1 and α-dH1 antibodies, József Mihály for the α-p94 antibody, the Drosophila Injection Service (HUN-REN Biological Research Centre) for generating CRISPR-Cas9 modified *Drosophila* lines, and the microscopy support provided by the Cellular Imaging Laboratory (HUN-REN Biological Research Centre). We are grateful to Zoltán Lipinszki, Albert Carbonell, Péter Görög, and the members of the DNA Damage and Nuclear Dynamics Research Group of the HUN-REN Biological Research Centre for their advice and technical assistance with the experiments presented in this study.

Conflicts of interest

The authors declare no conflict of interest.

Author contributions

RP and AP contributed to the investigation, methodology, and writing. LH contributed to the conceptualization, investigation, writing, and supervision. AS, BV, and BG contributed to the investigation. IMB and PV contributed to the data interpretation, revision of manuscript, and funding acquisition. ZV contributed to the conceptualization and funding acquisition. GT contributed to the conceptualization, supervision, funding acquisition, resources, and writing.

Peer review

The peer review history for this article is available at https://www.webofscience.com/api/gateway/wos/peer-review/10.1111/febs.70715.

Data availability statement

The data that support the findings of this study are openly available in figshare database at https://figshare.com/s/ea022f99e320c5e1696c.

References

1 Hergeth SP & Schneider R (2015) The H1 linker histones: multifunctional proteins beyond the nucleosomal core particle. *EMBO Rep* **16**, 1439–1453.
2 Fyodorov DV, Zhou B-R, Skoultchi AI & Bai Y (2018) Emerging roles of linker histones in regulating chromatin structure and function. *Nat Rev Mol Cell Biol* **19**, 192–206.
3 Allan J, Hartman PG, Crane-Robinson C & Aviles FX (1980) The structure of histone H1 and its location in chromatin. *Nature* **288**, 675–679.
4 Vyas P & Brown DT (2012) N- and C-terminal domains determine differential nucleosomal binding geometry and affinity of linker histone isotypes H10 and H1c. *J Biol Chem* **287**, 11778–11787.
5 Pérez-Montero S, Carbonell A & Azorín F (2016) Germline-specific H1 variants: the "sexy" linker histones. *Chromosoma* **125**, 1–13.
6 Pérez-Montero S, Carbonell A, Morán T, Vaquero A & Azorín F (2013) The embryonic linker histone H1 variant of drosophila, dBigH1, regulates zygotic genome activation. *Dev Cell* **26**, 578–590.
7 Nagel S & Grossbach U (2000) Histone H1 genes and histone gene clusters in the genus drosophila. *J Mol Evol* **51**, 286–298.
8 O'Farrell PH, Stumpff J & Tin Su T (2004) Embryonic cleavage cycles: how is a mouse like a Fly? *Curr Biol* **14**, R35–R45.
9 Sullivan W, Fogarty P & Theurkauf W (1993) Mutations affecting the cytoskeletal organization of syncytial *Drosophila* embryos. *Development* **118**, 1245–1254.
10 Takada S, Kelkar A & Theurkauf WE (2003) Drosophila checkpoint kinase 2 couples centrosome function and spindle assembly to genomic integrity. *Cell* **113**, 87–99.
11 Iampietro C, Bergalet J, Wang X, Cody NAL, Chin A, Lefebvre FA, Douziech M, Krause HM & Lécuyer E (2014) Developmentally regulated elimination of damaged nuclei involves a Chk2-dependent mechanism of mRNA nuclear retention. *Dev Cell* **29**, 468–481.
12 Henn L, Szabó A, Imre L, Román Á, Ábrahám A, Vedelek B, Nánási P & Boros IM (2020) Alternative linker histone permits fast paced nuclear divisions in early drosophila embryo. *Nucleic Acids Res* **48**, 9007–9018.
13 Izzo A & Schneider R (2016) The role of linker histone H1 modifications in the regulation of gene expression and chromatin dynamics. *Biochim Biophys Acta* **1859**, 486–495.
14 Andrés M, García-Gomis D, Ponte I, Suau P & Roque A (2020) Histone H1 post-translational modifications: update and future perspectives. *Int J Mol Sci* **21**, 5941.
15 Liao R & Mizzen CA (2016) Interphase H1 phosphorylation: regulation and functions in chromatin. *Biochim Biophys Acta Gene Regul Mech* **1859**, 476–485.

© 2026 The Author(s). *The FEBS Journal* published by John Wiley & Sons Ltd on behalf of Federation of European Biochemical Societies.

17424658, 0, Downloaded from https://febs.onlinelibrary.wiley.com/doi/10.1111/febs.70715 by HUN-REN Biological Research Center, Szeged, Wiley Online Library on [26/11/2026]. See the Terms and Conditions (https://onlinelibrary.wiley.com/terms-and-conditions) on Wiley Online Library for rules of use; OA articles are governed by the applicable Creative Commons License

16 Roque A, Ponte I, Arrondo JLR & Suau P (2008) Phosphorylation of the carboxy-terminal domain of histone H1: effects on secondary structure and DNA condensation. *Nucleic Acids Res* **36**, 4719–4726.
17 Roque A, Ponte I & Suau P (2017) Post-translational modifications of the intrinsically disordered terminal domains of histone H1: effects on secondary structure and chromatin dynamics. *Chromosoma* **126**, 83–91.
18 Roque A, Ponte I & Suau P (2016) Interplay between histone H1 structure and function. *Biochim Biophys Acta Gene Regul Mech* **1859**, 444–454.
19 Roque A, Ponte I & Suau P (2009) Role of charge neutralization in the folding of the carboxy-terminal domain of histone H1. *J Phys Chem B* **113**, 12061–12066.
20 Blumenfeld M (1979) Phosphorylated H1 histone in *Drosophila melanogaster*. *Biochem Genet* **17**, 163–166.
21 Villar-Garea A & Imhof A (2008) Fine mapping of posttranslational modifications of the linker histone H1 from Drosophila melanogaster. *PLoS One* **3**, e1553.
22 Bonet-Costa C, Vilaseca M, Diema C, Vujatovic O, Vaquero A, Omeñaca N, Castejón L, Bernués J, Giralt E & Azorín F (2012) Combined bottom-up and top-down mass spectrometry analyses of the pattern of post-translational modifications of *Drosophila melanogaster* linker histone H1. *J Proteomics* **75**, 4124–4138.
23 Siriaco G, Deuring R, Mawla GD & Tamkun JW (2015) A novel approach for studying histone H1 function in vivo. *Genetics* **200**, 29–33.
24 Zhai B, Villén J, Beausoleil SA, Mintseris J & Gygi SP (2008) Phosphoproteome analysis of *Drosophila melanogaster* embryos. *J Proteome Res* **7**, 1675–1682.
25 Laver JD, Marsolais AJ, Smibert CA & Lipshitz HD (2015) Regulation and function of maternal gene products during the maternal-to-zygotic transition in drosophila. *Curr Top Dev Biol* **113**, 43–84.
26 Tadros W & Lipshitz HD (2009) The maternal-to-zygotic transition: a play in two acts. *Development* **136**, 3033–3042.
27 Pérez-Roldán J, Henn L, Bernués J, Torras-LLort M, Tamirisa S, Belloc E, Rodríguez-Muñoz L, Timinszky G, Jiménez G, Méndez R *et al.* (2025) Maternal histone mRNAs are uniquely processed through polyadenylation in a stem-loop binding protein (SLBP) dependent manner. *Nucleic Acids Res* **53**, gkaf288.
28 Carbonell A, Henn L, Pérez-Roldán J, Tamirisa S, Szabó A, Boros IM & Azorín F (2020) In response to Li *et al.*: Linker histones function in *Drosophila* embryogenesis.
29 Li KK, Han D, Chen F, Li R, Zhou B-R, Bai Y, Yuan K & Rong YS (2019) Compensatory replacement of the BigH1 variant histone by canonical H1 supports normal embryonic development in Drosophila. *bioRxiv*.
30 Pehrson JR & Cole RD (1982) Histone H1 subfractions and H10 turnover at different rates in nondividing cells. *Biochemistry* **21**, 456–460.
31 Commerford SL, Carsten AL & Cronkite EP (1982) Histone turnover within nonproliferating cells. *Proc Natl Acad Sci USA* **79**, 1163–1165.
32 Rachdaoui N, Li L, Willard B, Kasumov T, Previs S & Sarkar D (2017) Turnover of histones and histone variants in postnatal rat brain: effects of alcohol exposure. *Clin Epigenetics* **9**, 117.
33 Mathieson T, Franken H, Kosinski J, Kurzawa N, Zinn N, Sweetman G, Poeckel D, Ratnu VS, Schramm M, Becher I *et al.* (2018) Systematic analysis of protein turnover in primary cells. *Nat Commun* **9**, 689.
34 Jukam D, Shariati SAM & Skotheim JM (2017) Zygotic genome activation in vertebrates. *Dev Cell* **42**, 316–332.
35 Climent-Cantó P, Carbonell A, Tamirisa S, Henn L, Pérez-Montero S, Boros IM & Azorín F (2021) The tumour suppressor brain tumour (brat) regulates linker histone dBigH1 expression in the drosophila female germline and the early embryo. *Open Biol* **11**, 200408.
36 Hendzel MJ, Lever MA, Crawford E & Th'ng JPH (2004) The C-terminal domain is the primary determinant of histone H1 binding to chromatin in vivo. *J Biol Chem* **279**, 20028–20034.
37 Contreras A, Hale TK, Stenoien DL, Rosen JM, Mancini MA & Herrera RE (2003) The dynamic mobility of histone H1 is regulated by cyclin/CDK phosphorylation. *Mol Cell Biol* **23**, 8626–8636.
38 Sarg B, Helliger W, Talasz H, Förg B & Lindner HH (2006) Histone H1 phosphorylation occurs site-specifically during interphase and mitosis. *J Biol Chem* **281**, 6573–6580.
39 Halmer L & Gruss C (1996) Effects of cell cycle dependent histone H1 phosphorylation on chromatin structure and chromatin replication. *Nucleic Acids Res* **24**, 1420–1427.
40 Lopez R, Sarg B, Lindner H, Bartolomé S, Ponte I, Suau P & Roque A (2015) Linker histone partial phosphorylation: effects on secondary structure and chromatin condensation. *Nucleic Acids Res* **43**, 4463–4476.
41 Rossetto D, Avvakumov N & Côté J (2012) Histone phosphorylation: a chromatin modification involved in diverse nuclear events. *Epigenetics* **7**, 1098–1108.
42 Hubner NC, Bird AW, Cox J, Splettstoesser B, Bandilla P, Poser I, Hyman A & Mann M (2010) Quantitative proteomics combined with BAC TransgeneOmics reveals in vivo protein interactions. *J Cell Biol* **189**, 739–754.
43 Waterhouse AM, Procter JB, Martin DMA, Clamp M & Barton GJ (2009) Jalview version 2--a multiple sequence alignment editor and analysis workbench. *Bioinformatics* **25**, 1189–1191.

© 2026 The Author(s). *The FEBS Journal* published by John Wiley & Sons Ltd on behalf of Federation of European Biochemical Societies.

17424658, 0, Downloaded from https://febs.onlinelibrary.wiley.com/doi/10.1111/febs.70715 by HUN-REN Biological Research Center, Szeged, Wiley Online Library on [26/11/2025]. See the Terms and Conditions (https://onlinelibrary.wiley.com/terms-and-conditions) on Wiley Online Library for rules of use; OA articles are governed by the applicable Creative Commons License

44 Port F, Chen H-M, Lee T & Bullock SL (2014) Optimized CRISPR/Cas tools for efficient germline and somatic genome engineering in drosophila. *Proc Natl Acad Sci USA* **111**, E2967–E2976.
45 Jeong J-Y, Yim H-S, Ryu J-Y, Lee HS, Lee J-H, Seen D-S & Kang SG (2012) One-step sequence- and ligation-independent cloning as a rapid and versatile cloning method for functional genomics studies. *Appl Environ Microbiol* **78**, 5440–5443.
46 Schindelin J, Arganda-Carreras I, Frise E, Kaynig V, Longair M, Pietzsch T, Preibisch S, Rueden C, Saalfeld S, Schmid B *et al*. (2012) Fiji: an open-source platform for biological-image analysis. *Nat Methods* **9**, 676–682.
47 Vujatovic O, Zaragoza K, Vaquero A, Reina O, Bernués J & Azorín F (2012) Drosophila melanogaster linker histone dH1 is required for transposon silencing and to preserve genome integrity. *Nucleic Acids Res* **40**, 5402–5414.
48 Cserpán I, Máthé E, Patthy A & Udvardy A (1997) Characterization of a drosophila phosphorylation-dependent nuclear-localization-signal-binding protein. *Biochem J* **328**, 821–826.

Supporting information

Additional supporting information may be found online in the Supporting Information section at the end of the article.

Fig. S1. Representative MS–MS fragmentation patterns of BigH1-derived phosphopeptides.

Fig. S2. Multiple sequence alignment of 12 Drosophila BigH1 proteins by MAFFT.

Fig. S3. Spatiotemporal expression pattern of wild-type and CRISPR-Cas9-modified mutant Drosophila embryos.

Fig. S4. Relative BigH1 mRNA levels over time. RT-qPCR analysis shows BigH1 mRNA levels measured in embryos of the indicated age derived from mothers of the specified genotypes.

Fig. S5. Immunostaining of control (BigH13F) and BigH1NPS nonphosphorylatable mutants.

Table S1. Evolutionary conservation of BigH1 phosphorylation sites.

© 2026 The Author(s). *The FEBS Journal* published by John Wiley & Sons Ltd on behalf of Federation of European Biochemical Societies.

17424658, 0, Downloaded from https://febs.onlinelibrary.wiley.com/doi/10.1111/febs.70715 by HUN-REN Biological Research Center, Szeged, Wiley Online Library on [26/11/2026]. See the Terms and Conditions (https://onlinelibrary.wiley.com/terms-and-conditions) on Wiley Online Library for rules of use; OA articles are governed by the applicable Creative Commons License